Scholte-wave azimuthal-anisotropic phase-velocity images in the near surface at Ekofisk from seismic noise correlations

Sjoerd de Ridder, Dave Nichols and Biondo Biondi

ABSTRACT

In this report we summarize work done on an ambient seismic noise recording made at the Ekofisk LoFS array. We first isolate the double frequency microseism noise and synthesize virtual seismic sources by cross-correlation. A dispersion analysis shows that these sources contain fundamental mode Scholte-waves. Using Eikonal tomography on the phase-delay times extracted by using the unwrapped instantaneous phase, we construct maps of Scholte wave phase-velocities and elliptical anisotropy. A high velocity anomaly is found in the center of the array, surrounded by a lower velocity region. Under the the southern end of the array we find higher velocities again. We retrieve azimuthal anisotropy that relates to the subsidence pattern.

AMBIENT SEISMIC FIELD RECORDED BY LOFS AT EKOFISK

Ekofisk has a Life of Field Seismic (LoFS) array installed over a large portion of the North Sea field. Figure 1 contains a map with station locations. The inline and crossline station spacings are approximately 50 m and 300 m respectively. We received a dataset spanning 41 hours, 28 minutes and 40 seconds starting October 24, 2011, UT 00:17:00. There is about 1 hour and 24 minutes of recording missing before noon on October 24. For 119 stations located in a radius of 750 m of UTM $(514, 6261)$ km (blue stations in Figure 1) we plot the spectral amplitudes over time in Figure 2. This spectagram is computed by Fourier transformation of 2.5-minute recording windows with 50% overlap. Below 0.15 Hz the hydrophone is dominated by ocean swells, which are wind generated gravity waves in the sea (Munk, 1950). These cause pressure variations on the sea floor, and when multiple swells constructively interfere they excite interface waves traveling along the sea-floor at double the frequency (Longuet-Higgins, 1950). This noise is therefore coined double frequency microseism noise. We observe the microseism noise between $0.35 - 1.35$ Hz. At frequencies above 1.5 Hz, a variety of predominantly field-operational noise sources dominates the recordings. This study focuses on the microseism noise because it travels along the sea-floor, and potentially provides subsurface information on the top hundreds of meters in the near surface immediately below the sea floor.

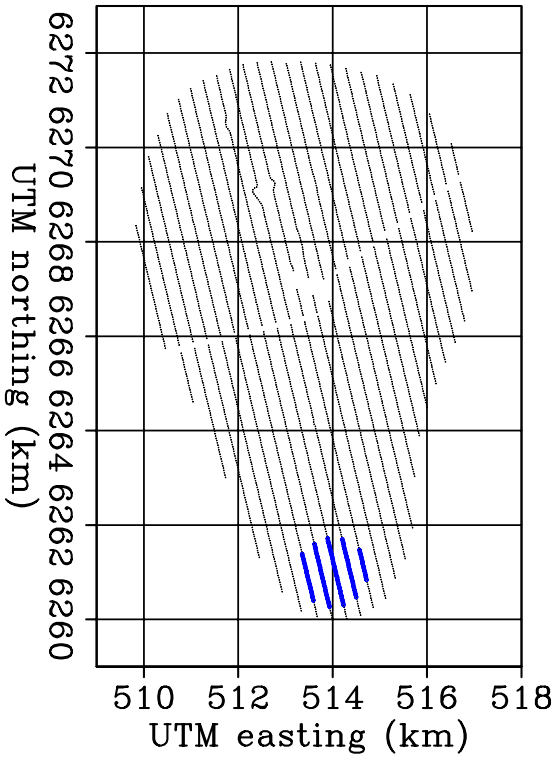

Figure 1: Map of station locations in the Ekofisk LoFS array. Each black dot denotes a station. The stations used to create the spectragram in Figure 2 and for the beamforming experiments in Figure 3 are blue. [**CR**]

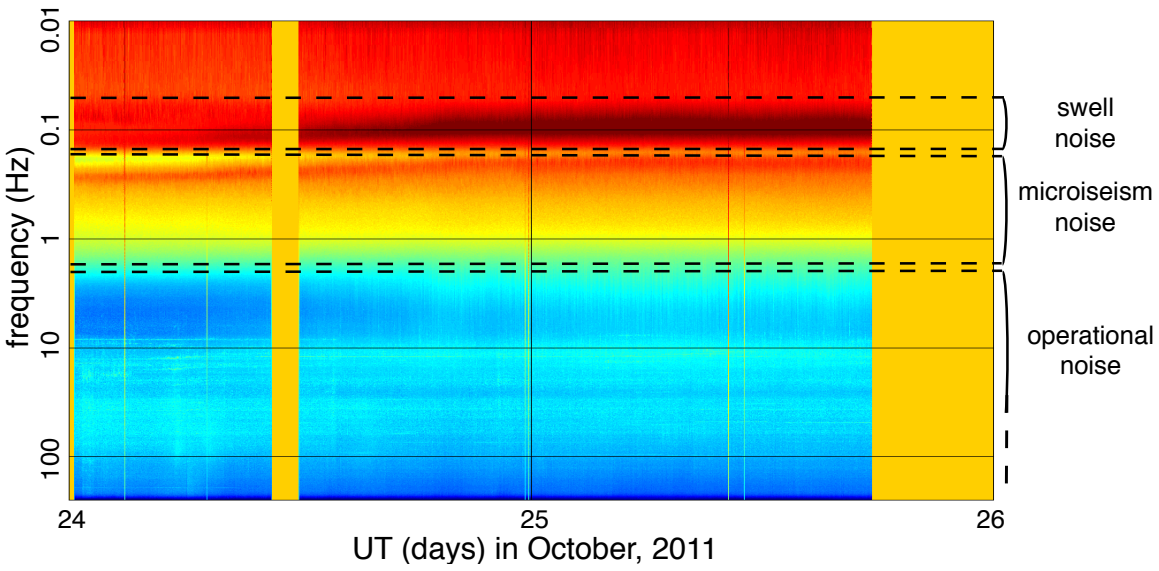

Figure 2: Spectragram showing spectral amplitudes versus time for the duration of the entire recording used in this study. [**CR**]

To investigate from which direction the ambient noise is incident at Ekofisk, we performed beamforming experiments for the same 119 stations used in the spectrogram calculation. First the recordings are bandpassed for energy between $0.55 - 0.65$ Hz and a slant stacked transforming the data to $\tau - p$ domain. We then average the result for 2.5 minutes and smooth with a triangle over 10 minutes. Figure 3 contains 13 snap shots, each 3 hours apart, from the beamforming experiment. High amplitudes (red) indicate the slowness and azimuth of incoming energy. Generally we observe a circle with absolute slowness $|\mathbf{s}| = 0.19$ ms/m, corresponding to a velocity of 525 m/s. These are the Scholte waves that travel in many directions composing the microseism noise of the ambient seismic field. Notice how the noise is remarkably omnidirectional.

VIRTUAL SOURCES FROM PASSIVE SEISMIC INTERFEROMETRY

Passive seismic interferometry is a technique that cross-correlates seismic recordings at two stations to form a signal, called the estimated Green's function (EGF), as if one of the stations were a seismic source (Claerbout, 1968; Rickett and Claerbout, 1999; Schuster et al., 2004; Wapenaar and Fokkema, 2006). Cross-correlations of passive seismic recordings between all possible station pairs in an array then creates a full virtual seismic survey, $\mathbf{D}(\omega, x_r, x_s)$:

$$\mathbf{D}(\omega, x_r, x_s) = \mathbf{r}(\omega, x_r)\ \mathbf{r}(\omega, x_s)^{\dagger}, \tag{1}$$

where $\mathbf{r}(\omega, x)$ is a vector containing passive seismic recordings at all stations, and $\dagger$ denotes complex conjugation and transposition. By cross-correlating different components of particle velocity we can retrieve all elements of the Green's matrix (Wapenaar and Fokkema, 2006). The cross-correlation signal contains the causal Green's function and its anti-causal reciprocal counter part. However, this technique is valid only when the energy in the ambient seismic field satisfies a condition known as energy equipartioning. In practice, this requirement limits the application of seismic interferometry to certain frequency regimes. The ambient seismic field at low frequencies ($0.5 - 1.3$ Hz) is dominated by the double-frequency microseism peak, a source of seismic energy that satisfies the requirement of energy equipartitioning and can be utilized for seismic interferometry (Stewart, 2006; Dellinger and Yu, 2009). The causal Green's function and its anti-causal reciprocal counter part should be an even signal (the cross-correlation signal should be purely real-valued). The anti-symmetric part of the cross-correlation signal reflects deviations from the assumption of energy equipartitioning.

The recorded data in the hydrophone component was filtered using a frequency domain taper with a flat response for 0.4-1.3 Hz, and as a Hann-taper extending from 0.35 Hz to 1.35 Hz. The data was then cross-correlated in 10 blocks of 4 hours. These cross-correlations where then stacked to result in a virtual seismic survey with sources and receivers at all stations in Ekofisk's LoFS array. Figure 4 contains an example

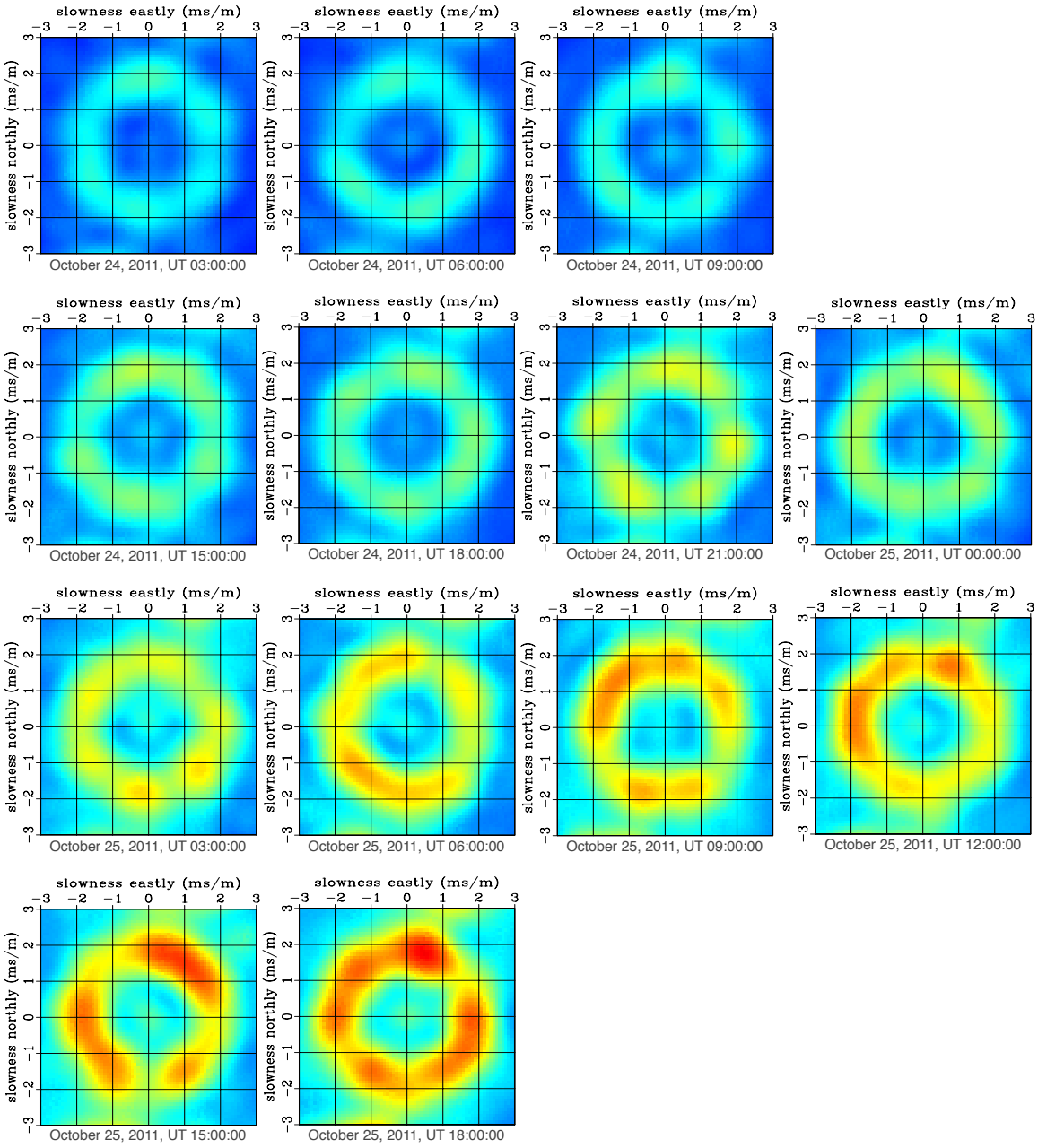

Figure 3: Beamform experiments for recorded data between $0.55 - 0.65$ Hz. Frames are generally 3 hours apart (except for missing data) and they indicate the slowness and azimuth of incoming surface wave energy. [**CR**]

of a virtual seismic source in vertical component of particle velocity. Figures 4a to e contain the symmetric part of the cross-correlation signal, while Figures 4f to j contain the asymmetric part. There is very little coherent energy in the asymmetric part and the correlation fluctuations in the asymmetric part are of the order of the background fluctuations in the symmetric part. This indicates that the microseism noise at Ekofisk is very suitable for seismic interferometry.

A dispersion image is calculated as the amplitude in the Radon $(\omega - p)$ domain, balanced over frequencies. The dipserison image calculated using all offsets with midpoints between UTM $(513 - 514, 6269 - 6270)$ km is shown in Figure 5. The fundamental-mode Scholte waves are clearly visible. It is a dispersive wavemode, i.e. the wavespeed varies with frequency.

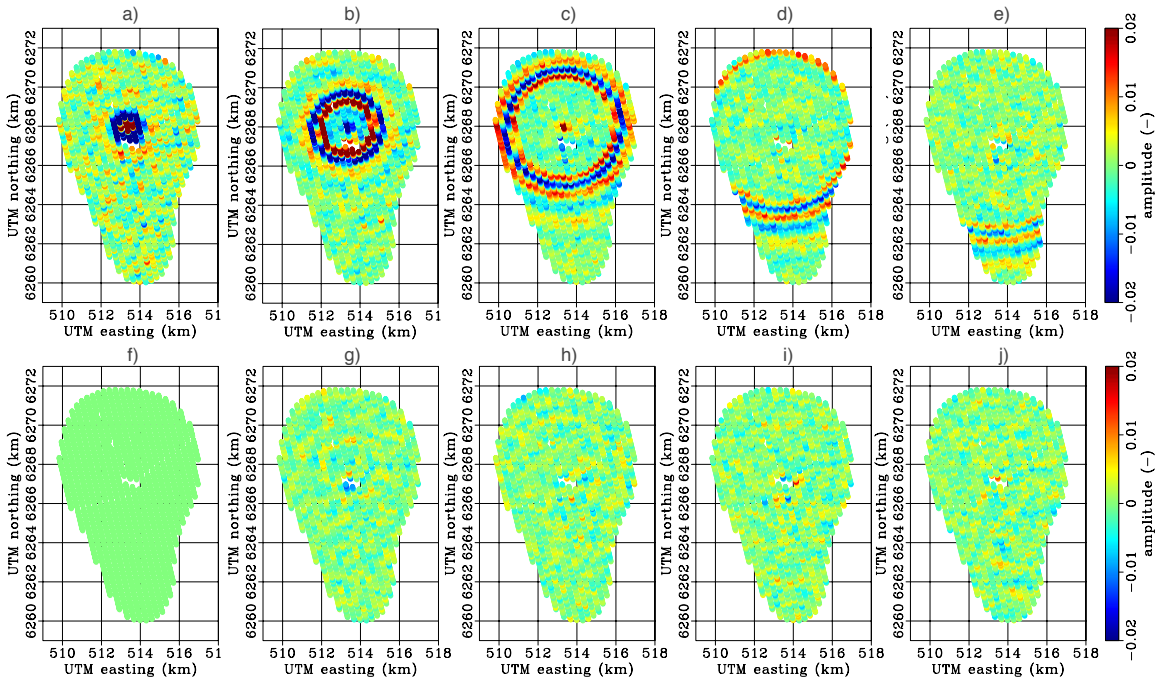

Figure 4: Snap shots for even (a-e) and odd (f-j) part of the virtual seismic sources. At correlation lags: 0s (a and f), 4s (b and g), 8s (c and h), 12s (d and i), and 16s (e and j). [**CR**]

AZIMUTHAL-ANISOTROPIC EIKONAL TOMOGRAPHY FOR PHASE VELOCITY USING THE INSTANTANEOUS PHASE

The surface waves emitted by the virtual seismic sources propagate along the seafloor with wavelengths between 1100 m at 0.5 Hz and 375 m at 1.2 Hz (from Figure 5). These long wavelengths provide sensitivity away from the seabed (thus in depth), and different frequencies will be sensitive differently with depth. Therefore, we are

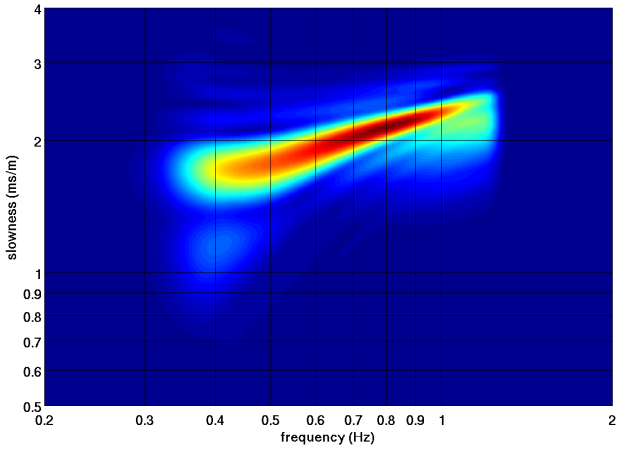

Figure 5: Dispersion image for the virtual seismic sources. [**CR**]

interested in creating phase velocity maps, showing the velocities as a function of space for a given frequency. We thus need to measure the apparent traveltime for a Scholte-wave for a given frequency; phase-delay times.

Aki and Richards (2002) showed that the fundamental mode Scholte wave Green's functions in the far field behave like:

$$G(\mathbf{x}_r, \mathbf{x}_s) \propto \exp\left[-i\left(\frac{\omega}{c(\omega)}|\mathbf{x}_s - \mathbf{x}_r| + \pi/4\right)\right]. \tag{2}$$

If we take the instantaneous phase of the cross-correlations and add a $\frac{\pi}{4}$ phase shift, we find a phase-function that should be proportional to $\omega\frac{|\mathbf{x}_s-\mathbf{x}_r|}{c(\omega)}$. Thus it makes sense to define the phase-delay time that given a phase velocity $c(\omega)$ is a linear function of source-receiver distance, $\tau(\omega) = \frac{|\mathbf{x}_s-\mathbf{x}_r|}{c(\omega)}$. This phase-delay time represents a traveltime for Scholte waves at a particular frequency.

Eikonal tomography is a technique that evaluates the Eikonal equation on traveltime surfaces to directly find slowness estimates. Both Lin et al. (2009) and Mordret et al. (2013) use an isotropic Eikonal equation to estimate the azimuthal-anisotropic local slowness of wave-propagation. A disadvantage of that method is that the observed azimuth of fast and slow directions cannot easily be regularized over space. Here I propose a different approach.

I assume the fundamental mode Scholte waves exhibit elliptical anisotropy, such that velocity can be expressed as:

$$V^2(\phi) = V_f^2\,\cos^2(\phi-\alpha) + V_s^2\,\sin^2(\phi-\alpha), \tag{3}$$

where V_f and V_s are the maximum and minimum velocities (for V over all angles ϕ) and α is the fast direction of velocity. This velocity is plugged into the dispersion relation:

$$-\omega^2 = V^2(\phi)\left[k_x^2 + k_y^2\right], \tag{4}$$

defining a frequency domain equation:

$$-\omega^2 U(\mathbf{x},\omega) = \left[(V_f^2 - V_s^2)\cos^2(\alpha) + V_s^2\right] \partial_x^2 U(\mathbf{x},\omega) + \tag{5}$$

$$2\left[(V_f^2 - V_s^2)\cos(\alpha)\sin(\alpha)\right] \partial_x\partial_y U(\mathbf{x},\omega) + \tag{6}$$

$$\left[(V_f^2 - V_s^2)\sin^2(\alpha) + V_s^2\right] \partial_y^2 U(\mathbf{x},\omega). \tag{7}$$

To derive an appropriate Eikonal equation, we plug the test function, $U(\mathbf{x},\omega) = A(\mathbf{x},\omega)\exp\{-i\omega\ T(\mathbf{x},\omega)\}$, into equation 7 and collect the leading terms (in ω^2) to find:

$$1 = \left[\begin{array}{cc} \partial_x T(\mathbf{x},\omega) & \partial_y T(\mathbf{x},\omega) \end{array}\right] \left[\begin{array}{cc} M_{11} & M_{12} \\ M_{12} & M_{22} \end{array}\right] \left[\begin{array}{c} \partial_x T(\mathbf{x},\omega) \\ \partial_y T(\mathbf{x},\omega) \end{array}\right]. \tag{8}$$

For the matrix elements we have

$$M_{11} = (V_f^2 - V_s^2)\cos^2(\alpha) + V_s^2 \tag{9}$$

$$M_{12} = (V_f^2 - V_s^2)\cos(\alpha)\sin(\alpha) \tag{10}$$

$$M_{22} = (V_f^2 - V_s^2)\sin^2(\alpha) + V_s^2. \tag{11}$$

The eigenvalues of the matrix $\mathbf{M}$ are V_f^2 and V_s^2, and the tangent of the eigenvectors indicate the fast and slow directions. One mayor advantage of this approach is that the elements of this matrix can be regularized over space.

The easterly and northerly derivatives are calculated by simple centered finite difference on a phase-delay time map interpolated by splines (Sandwell, 1987) to a grid of 100 m by 100 m. We invert for the matrix $\mathbf{M}$ using an L_1 norm of the logarithm of equation 8 (after discarding outliers of measurements of derivatives). The matrix M is regularized over space using a Laplacian. Figure 6 provides an schematic overview of the input of Eikonal tomography for two sources.

Phase-delay times are plotted in Figures 6a and 6d. Easterly derivatives of the interpolated phase-delay times are shown in Figures 6b and 6e and northerly derivatives of the interpolated phase-delay times are shown in Figures 6c and 6f.

We construct maps of elliptical anisotropic Scholte-wave phase-velocities for each frequency. Figure 7 contain maps of Scholte-wave phase velocity at 0.5 Hz to 1.3 Hz. The colors depict the isotropic component, $V_0 = (V_f + V_s)/2$. The azimuth of the dashes denote the fast direction of anisotropy. The length of the dashes indicate the magnitude of anisotropy, $dV = (V_f - V_s)/2$, as a fraction of the isotropic component. The dash in the upper-right corner of each plot denotes a anisotropic magnitude of 10%. For comparison the bathymetry is included through blue contour lines with a 2 m interval. For some frequencies it is hard to distinguish an interpretable pattern in the anisotropy. However, for the Scholte wave phase velocities at 1.0 Hz we observe a pattern that relates to the seafloor subsidence. In addition, we generally find higher Scholte-wave velocities where the sea-floor curvature is low, and lower Scholte-wave velocities where the sea-floor curvature is high. The edge of high velocities at the

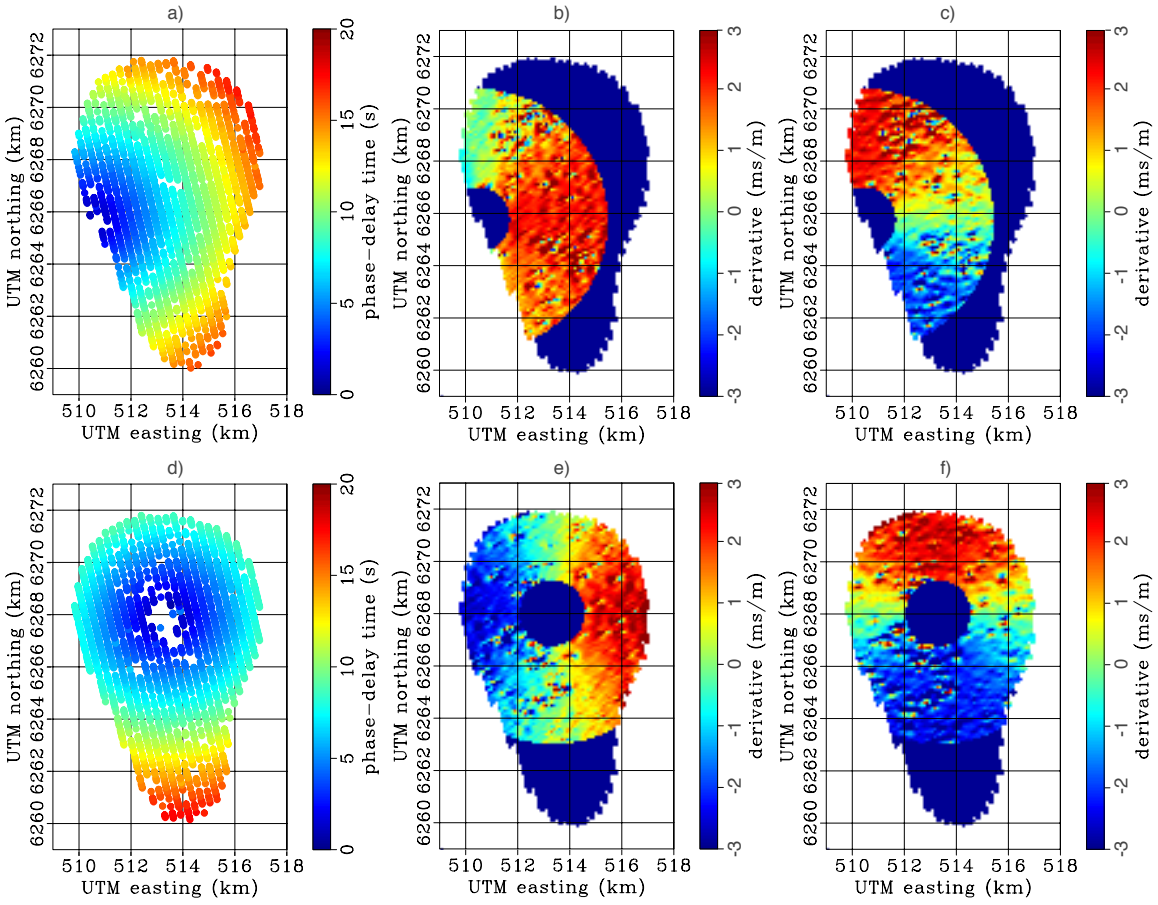

Figure 6: Schematic of frequency-domain Eikonal tomography. Phase delay times at 1.0 Hz for two virtual seismic sources (a and d). Easterly derivatives (b and e) and northerly derivatives (c and f) of the interpolated phase-delay surfaces. [**CR**]

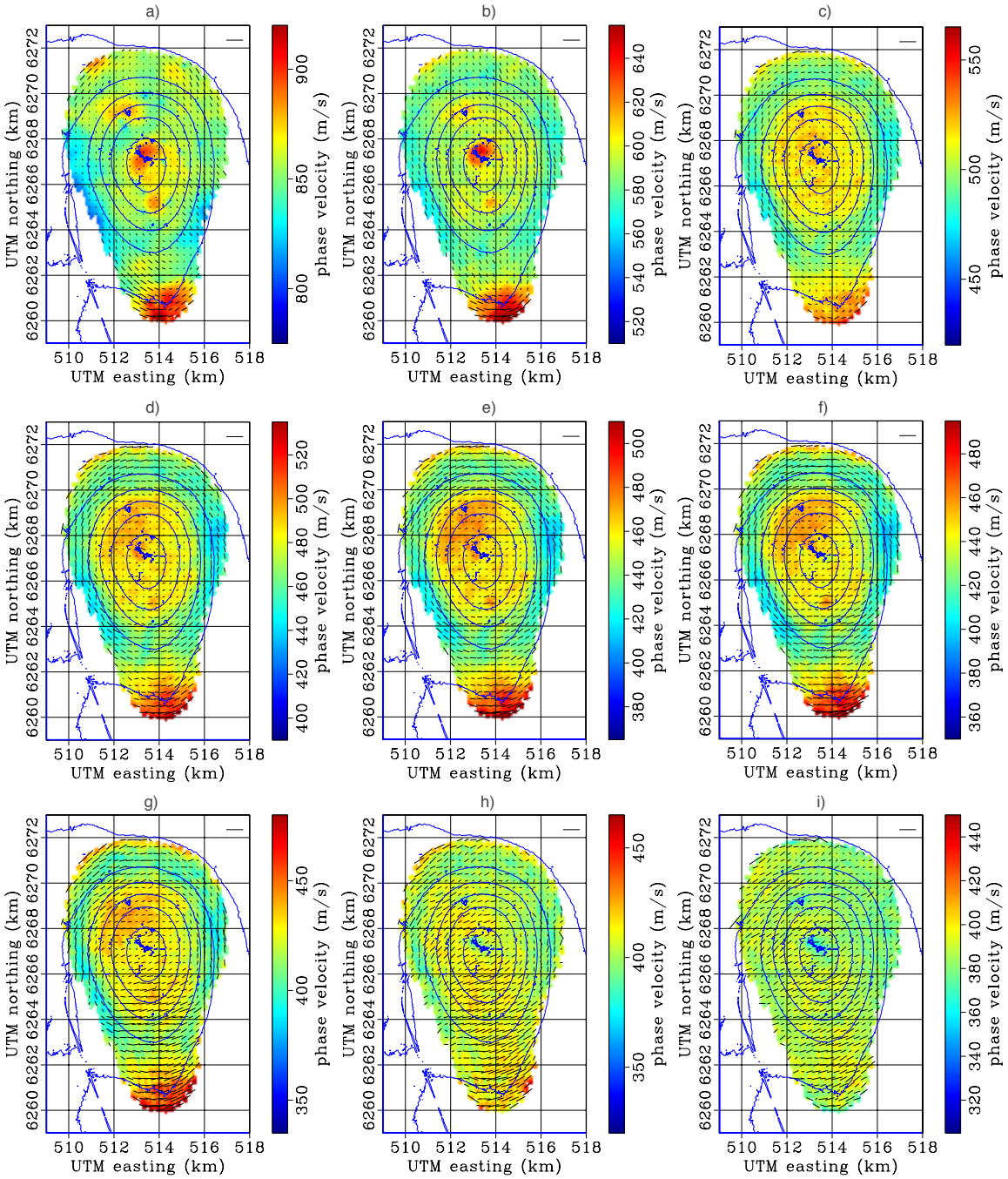

Figure 7: Scholte wave phase-velocities for 0.5 Hz (a), 0.6 Hz (b), 0.7 Hz (c), 0.8 Hz (d), 0.9 Hz (e), 1.0 Hz (f), 1.1 Hz (g), 1.2 Hz (h), 1.3 Hz (i). The colors depict the isotropic component. The azimuth of the dashes denote the fast direction anisotropy. The length of the dashes indicate the magnitude of anisotropy as a fraction of the isotropic component. The dash in the upper-right corner of each plot denotes a anisotropic magnitude of 10%. The bathymetry is included by blue contour lines with a 2 m interval. [**CR**]

northern edge of the recovered map, may be an extrapolation artifact but may also be the rim of the subsidence pattern.

For dispersive interface waves, lower frequencies generally relate to deeper regions (Aki and Richards, 2002). When we arrange maps of phase velocity for a set of frequencies as a cube with frequency as vertical axis, we find a phase-velocity cube (ω, x, y) that forms a first order image of Scholte waves in the top few 100 m of the near surface. Figure 8 contains three slices through this cube. Notice how the generally higher velocities in the center of the subsidence pattern reach to extend all the way to the lowest frequencies. We notice a significant high velocity region in the very center of the array at very low frequencies.

SUMMARY

In this report it is shown that the low frequency ambient seismic field as recorded by the Ekofisk LoFS array is suitable for retrieval of Scholte waves by seismic interferometry. In fact, the microseism energy at Ekofisk in this recording is very uniformly distributed over azimuth, and thus ideal for seismic interferometry. However, different recordings have different characteristics because noise characteristics are transient with time. Using a tomographic method based on evaluating the Eikonal equation over a phase delay-time surface, we recover a phase velocity map for 1.0 Hz. A high velocity anomaly is found in the center of the array, surrounded by a lower velocity region. Under the the southern end of the array we find higher velocities again. We retrieve azimuthal anisotropy that relates to the subsidence pattern.

ACKNOWLEDGMENTS

ConocoPhillips Skandinavia AS and the PL018 Partnership (Total E&P Norge AS, ENI Norge AS, Statoil Petroleum AS and Petoro AS) for access to Ekofisk data, and permission to publish these results. Olaf Knoth, Ali Tura, Alexandre Bertrand and Roman Kazinnik for helpful discussions and suggestions.

REFERENCES

Aki, K., and P. G. Richards, 2002, Quantitative Seismology - second edition: University Science Books.

Claerbout, J. F., 1968, Synthesis of a layered medium from its acoustic transmission response: Geophysics, **33**, 264–269.

Dellinger, J. A., and J. Yu, 2009, Low-frequency virtual point-source interferometry using conventional sensors: 71st Meeting, European Associated of Geoscientists and Engineers, Expanded Abstracts, X047.

Lin, F. C., M. H. Ritzwoller, and R. Snieder, 2009, Eikonal tomography: surface

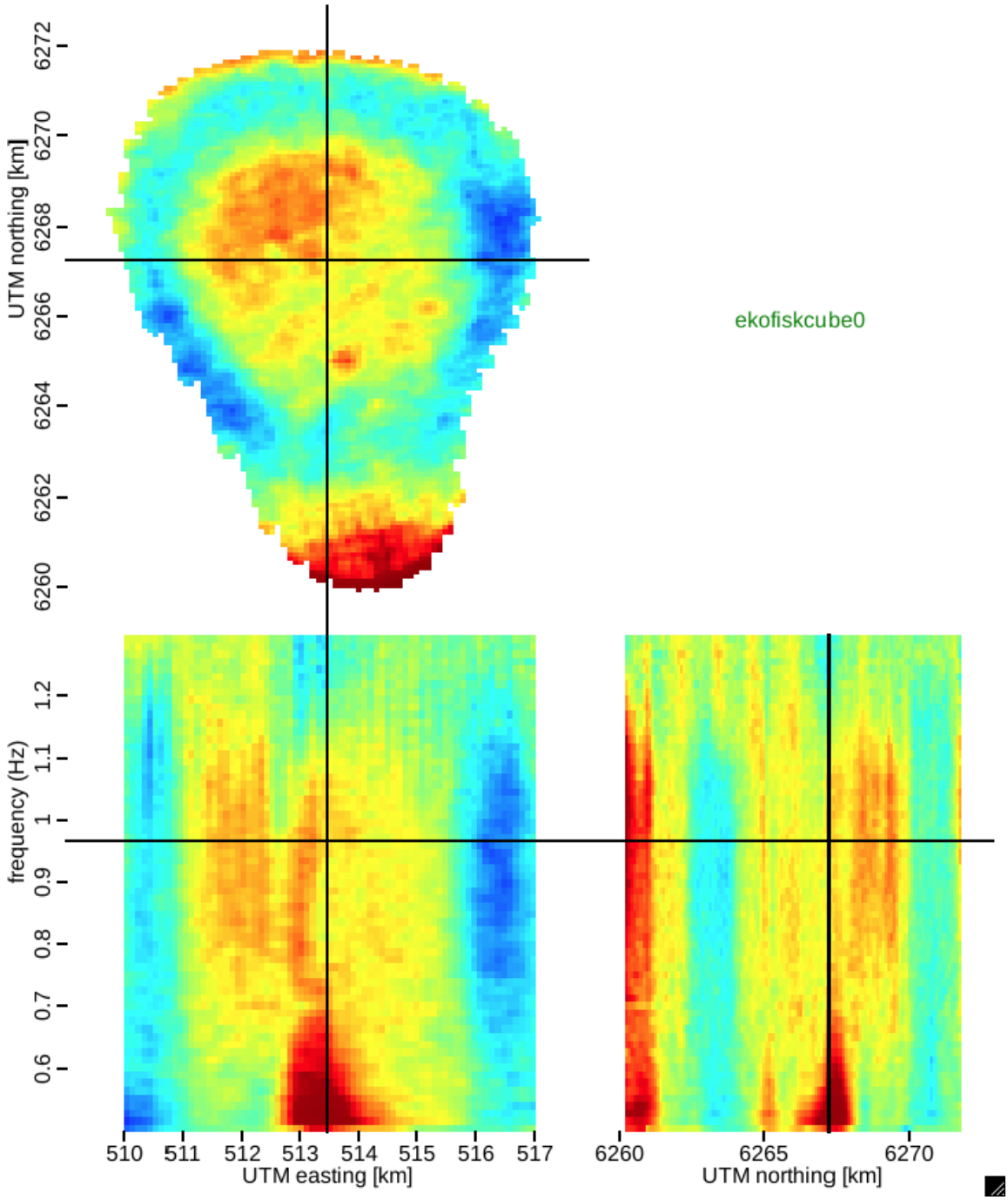

Figure 8: Cube of the isotropic part of Scholte wave velocities, (ω, x, y). [**NR**]

wave tomography by phase front tracking across a regional broad-band seismic array: Geophys. J. Int., **177**, 1091–1110.

Longuet-Higgins, M. S., 1950, A theory of the origin of microseisms: Phil. Trans. R. Soc. Lond. A, **243**, 135.

Mordret, A., N. Shapiro, S. Singh, P. Roux, and O. Barkved, 2013, Helmholtz tomography of ambient noise surface wave data to estimate scholte wave phase velocity at valhall life of the field: GEOPHYSICS, **78**, WA99–WA109.

Munk, W. H., 1950, Origin and generation of waves: Proceedings 1st International Conference on Coastal Engineering, 1–4.

Rickett, J., and J. Claerbout, 1999, Acoustic daylight imaging via spectral factorization: Helioseismology and reservoir monitoring: The Leading Edge, **18**, 957–960.

Sandwell, D. T., 1987, Biharmonic spline interpolation of GEOS-3 and SEASAT altimeter data: Geophys. Res. Let., **14**, 139–142.

Schuster, G. T., J. Yu, J. Sheng, and J. Rickett, 2004, Interferometric/daylight seismic imaging: Geophys. J. Int., **157**, 838–852.

Stewart, P., 2006, Interferometric imaging of ocean bottom noise: SEG Technical Program Expanded Abstracts, **25**, 1555–1559.

Wapenaar, K., and J. Fokkema, 2006, Green's function representations for seismic interferometry: Geophysics, **71**, SI33–SI46.